# MULTICYCLIC VIBRATION CONTROL OF A HELICOPTER ROTOR WITH ACTIVE TWIST ACTUATION

Do-Hyung Kim, dhkim@kari.re.kr, Korea Aerospace Research Institute (Republic of Korea)

Seonghyun Hong, hsh721@naver.com, Konkuk University (Republic of Korea)

Sung N. Jung, snjung@konkuk.ac.kr, Konkuk University (Republic of Korea)

**Abstract**

The vibration control performance of a Mach scaled Bo-105 rotor is evaluated using active twist multicyclic control. The simulation data for the baseline flight condition are generated using CAMRAD II. A linear, quasi-static, frequency domain model with up to six multicyclic higher harmonic control inputs and twelve harmonic response outputs of nonrotating hub loads are identified offline by the least squared error estimate. The optimal control input for minimizing the quadratic performance function along with the output response to the optimal control are calculated. The vibration reduction performances with the obtained optimal control input are calculated. The single harmonic control results show close agreement with the low vibration conditions by the amplitude and phase sweep method. When multicyclic control is applied, vibration reduction performance is improved compared to single harmonic control, and nonrotating hub vibration is reduced by up to 64%. A coupling of MATLAB and CAMRAD II is introduced to evaluate closed-loop multicyclic control systems. The coupled closed-loop analysis result shows good agreement with the simulation result using identified linear system model. The closed-loop control using the gradient descent algorithm shows very good vibration reduction performance and the reduced vibration level converges to the optimal solution.

## 1. INTRODUCTION

There have been a number of numerical and experimental research activities on active rotor control systems for helicopter vibration reduction. Higher Harmonic Control (HHC) has been successfully applied to reduce vibration and noise [1]. Although HHC demonstrated its capabilities to reduce vibrations and noise, other active control methods were investigated more and more. The main drawback of HHC is the limitation of control frequencies, and the fact that noise and vibrations could often not be reduced at the same time [2]. The most promising alternative to HHC is Individual Blade Control (IBC) [3]. Many IBC concepts have been designed and tested; active pitch rods [4], active trailing edge flap [5, 6], active twist [7, 8, 9], active tab [10], active Gurney flaps, and so on.



Among them, active trailing edge flap has been extensively studied and successfully applied to flight tests. Ref. 6 showed a successful vibration reduction performance up to 80% on an experimental BK117 airframe using the active flaps with time domain control algorithm. However, additional mechanical parts are necessary to implement trailing edge flap actuators in the blades. On the other hand, the active twist concept based on the strain-induced actuation does not need additional mechanical parts.

Piezoelectric active fiber composite (AFC) or macro fiber composite (MFC) has been utilized for actuators of small-scaled active twist rotors. These actuators produce the strain-induced twisting when excited by electric fields. Active Twist Rotor (ATR) based on AFC showed fixed-system vibratory loads reduction of 60% to 95% at the wind tunnel test in the NASA Langley Transonic Dynamics Tunnel (TDT) [7]. However, control mode was open-loop and excitation frequency was single harmonic. Control phase sweep has been done for 3P (3/rev), 4P, and 5P actuation frequencies with several control amplitudes. Then, the best actuation frequency, amplitude, and control phase could be identified.

A study on active twist rotors with MFC actuators has been performed at the German Aerospace Center (DLR) since 1995 [11]. Since 2009, it has been expanded as an international cooperation project, Smart Twisting Active Rotor (STAR). During the preliminary test, a fatigue problem occurred in the MFC actuator, and the cause of failure was investigated [12] and the actuator and rotor blade



Presented at 47th European Rotorcraft Forum, United Kingdom, 7-9th September, 2021

designs was improved [13]. Since then, new STAR blades are being fabricated and wind tunnel tests are in preparation.

Regarding the twist actuation for vibration reduction, most widely used approaches are based on harmonic excitation. For single harmonic control, amplitude and phase sweeps are performed at several harmonic frequencies. Then the best control input frequency, amplitude, and control phase could be identified by selecting the best performance case among the results. This method can be extended to multiple harmonic actuation. Active twist actuation with multiple harmonics has been applied to simulation studies of performance improvement, and vibration and noise reduction [14, 15]. While multiple harmonics provide a wide range of harmonic inputs to extend the control authority over single harmonic control, the complexity can be increased due to the large design space. Another approach is a non-harmonic type of twist actuation. A step input characterized by azimuthal position to start, duration, and magnitude was applied for noise reduction [16]. And Ref. 17 showed that an advancing-side-only actuation with 2P harmonic input was effective in performance enhancement. And the study on the best actuation scenario search using a particle swarm genetic algorithm for performance improvement and vibration reduction with simple harmonic input and segmented step function is discussed in Ref. 18.

In general, it is expected that better performance will be obtained when a multiple harmonic or non-harmonic control method is applied compared to a single harmonic control. On the other hand, when a multiple harmonic or non-harmonic control technique is applied, the amount of calculation for obtaining an optimal solution may be greatly increased depending on the algorithm. However, when the helicopter vibration characteristics are linear, the optimal control input can be derived through relatively few calculations by applying the optimal control technique. In addition, this optimal control technique can be effectively used when designing a feedback controller by processing flight test data. A class of algorithms for the multicyclic control of helicopter vibration is already derived and discussed in Ref. 19. And a numerical simulation study using the various regulator types are has been performed and discussed in Ref. 20. Multicyclic vibration control is based on a linear, quasi-static, frequency domain representation of the helicopter model. Optimal control solution for minimizing the quadratic performance function can be calculated by simple linear algebra. And it can be implemented in the form of an open-loop or a closed-loop control system.

In the present study, vibration control performance when multicyclic control technique is applied to a dynamically scaled Bo-105 rotor is evaluated and discussed. CAMRAD II calculation data for the descent flight condition is used as the basis for controller configuration. A linear, quasi-static, frequency domain models with up to 6 multicyclic input and 12 harmonic response output of nonrotating hub loads are used for representing the helicopter models. The offline system identification is applied to obtain the helicopter model by least squared error. The optimal control input for minimizing the quadratic performance function and corresponding response to the optimal control are calculated. A nondimensionalized vibration index is defined and used to combine 12 nonrotating hub load components to represent vibration reduction performance in a single number. Open-loop control performance is simulated by CAMRAD II calculation with the optimal control input. Then gradient descent method is utilized for closed-loop control, and the performance is simulated by MATLAB/CAMRAD II coupled analysis.

## 2. MULTICYCLIC VIBRATION CONTROL

Multicyclic vibration control system is schematically shown in Figure 1. The objective is to minimize vibration on the rotating or nonrotating components. In steady state flight, the helicopter vibratory loads are periodic, with fundamental frequency 1P (1/rev, once per revolution) in the rotating frame and NP (N/rev) for components in the nonrotating frame, where N is the number of blades. Hence the control required to alleviate the vibration will be periodic, and the control system can deal with the harmonics of the input and output [19]. Harmonic analysis of the response of the helicopter is required to provide harmonics of vibration to the controller, and the time domain signal of the control command should be constructed and provided to the actuators, and the dynamics of the actuators should also be considered. In order to focus on the vibration control performance

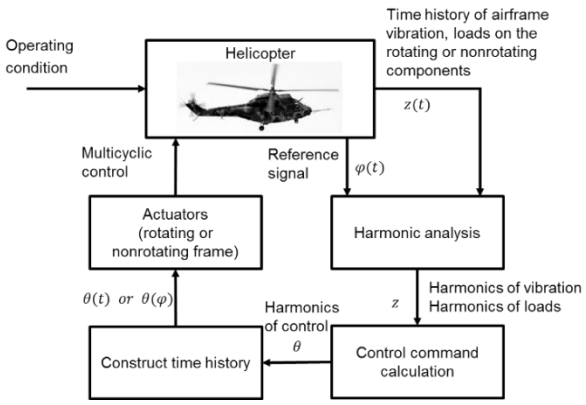


Figure 1. Schematic of multicyclic vibration control system.



Presented at 47th European Rotorcraft Forum, United Kingdom, 7-9th September, 2021

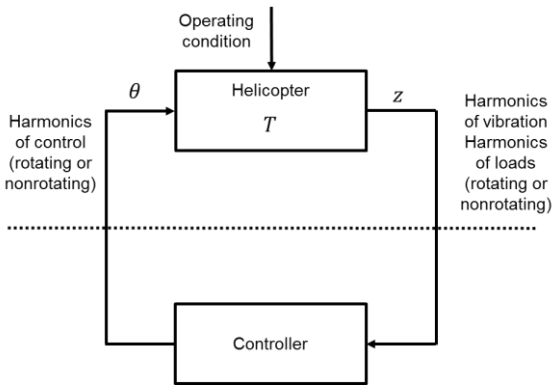


Figure 2. Simplified schematic of multicyclic vibration control system.

of a multicyclic controller, the components except the controller can be simplified to a helicopter system as shown in Figure 2.

## 2.1. System Model

The helicopter is represented by a linear, quasi-static frequency domain model relating the output $z$ to the input $\theta$ through a transfer function at $t_n = n\Delta t$. Here $z$ is a vector of the sine and cosine components of the harmonics of the vibration, in either the rotating or the nonrotating frame. The input $\theta$ is a vector of the harmonics of the multicyclic control, in either the rotating or nonrotating frame. $T$ is the transfer function, and the subscript $n$ represent *n*-th step. The sampling time-step $\Delta t$ must be long enough for transients to die out for the harmonics to be measured. Typically, this requires an interval of at least one rotor revolution [19]. Two types of models are used to represent mathematically the multicyclic control system. One is the local model that is linear about the current control value, and the other is the global model that is linear over the entire range of control. In the present study, only the simulation of the global model was performed. The global model is represented as follows:

(1) $$z_n = z_0 + T\theta_n$$

The transfer function $T$ and the uncontrolled response $z_o$ depend on the operating condition defined by the rotor lift, propulsive force, and forward speed at least.

## 2.2. Offline System Identification

System identification is the process of constructing a numerical model $\hat{T}$ for the helicopter model $T$ as shown in Figure 3.

Offline identification implies constant parameter. A set of *N* measurements is made using a prescribed schedule of control inputs. The minimum number of

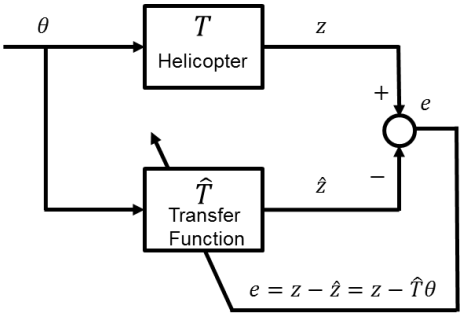


Figure 3. System identification.

independent measurements required is equal to the number of control input. Error is defined as the difference between the measured and the estimated responses.

(2) $$e = z - \hat{z} = z - \hat{T}\theta$$

where, $z$ is the measured response and $\hat{z}$ is the estimated response. With *N* measurements set, the error matrix *E* containing *N* columns of error vector can be represented as

(3) $$E = Z - \hat{T}\Theta$$

where, $Z$ is the response matrix which contains *N* columns of measurements $z$, and $\Theta$ is the multicyclic input matrix which contains *N* columns of control input $\theta$. Offline system identification can be done by the method of least squares. Consider the squared sum of the *j*-th row of the error matrix.

(4) $$S_j = e_j e_j^T = \sum_{n=1}^{N} \left(z_{jn} - t_{jn}\theta_n\right)^2 = \left(z_j - t_j\Theta\right)\left(z_j - t_j\Theta\right)^T (n = 1, \dots, N)$$

where, the subscript $j$ corresponds to the sensor number. $e_j$ is the *j*-th row of the error matrix E, $z_j$ is the *j*-th row of the response matrix *Z*, and $t_j$ is the *j*-th row of the transfer function $\hat{T}$. The solution $t_j$ that minimize $S_j$ can be found by $\partial S_j / \partial t_j = 0$.

(5) $$t_j = z_j\Theta^T(\Theta\Theta^T)^{-1}$$

The transfer function model $\hat{T}$ is a collection of all the solutions for $t_j$.

(6) $$\hat{T} = Z\Theta^T(\Theta\Theta^T)^{-1}$$

## 2.3. Optimal Control Solution

The control algorithm is based on the minimization of the performance function. The quadratic performance function used in this study is

(7) $$J = z_n^T W_z z_n + \theta_n^T W_\theta \theta_n + \Delta\theta_n^T W_{\Delta\theta} \Delta\theta_n$$



Presented at 47th European Rotorcraft Forum, United Kingdom, 7-9th September, 2021

where, $\Delta\theta_n = \theta_n - \theta_{n-1}$, $W_z$ is the weighting matrix for the response, $W_\theta$ is the weighting matrix for the multicyclic control input, and $W_{\Delta\theta}$ is the weighting matrix for the multicyclic control rate. Typically the weighting matrices are diagonal, and have the same value for all harmonics of a particular quantity. Then $J$ is a weighted sum of the mean squares of the vibration and control. The optimal control input to alleviate the helicopter vibration is found by substituting for $z_n$ in the performance function, and then solving for $\theta_n$ that minimize $J$. Setting $\partial J/\partial\theta_n = 0$ and using $\partial z_n/\partial\theta_n = T$ gives:

(8) $$T^T W_z z_n + W_\theta \theta_n + W_{\Delta\theta}\Delta\theta_n = 0$$

Substituting equation (1) into equation (8) gives:

(9) $$\theta_n = C z_0 + C_{\Delta\theta}\theta_{n-1}$$

where, $C = -DT^T W_z$, $C_{\Delta\theta} = DW_{\Delta\theta}$, and $D = (T^T W_z T + W_\theta + W_{\Delta\theta})^{-1}$. General solution that applies to both the local and global models can be found in Ref. 19, which is as follows:

(10) $$\theta_n = C z_{n-1} + (C_{\Delta\theta} - CT)\theta_{n-1}$$

### 2.4. Open-loop Control

The optimal solution for the global model (equation (9)) defines an open-loop control determined by the uncontrolled response $z_0$ and the previous control input $\theta_{n-1}$. There is no feedback of the measured response. When $W_{\Delta\theta} = 0$, the open-loop control solution reduces to

(11) $$\theta_n = C z_0$$

The control input is independent of the previous control input and is determined only by the uncontrolled response $z_0$. The open-loop control is not applicable to the local model of the helicopter.

### 2.5. Closed-loop Control

The optimal solutions for the both the global and local models defines a closed-loop control obtained by feedback of the measured response $z_{n-1}$. For the global model with no estimation error, that is $\hat{T} = T$, no measurement noise, and $W_{\Delta\theta} = 0$, the control command converges to the optimal solution in one cycle. If there is small amount of measurement noise, equation (10) will act as a closed-loop controller.

Practical method of implementing a closed-loop controller to minimize quadratic performance function is a gradient descent. Gradient descent is an optimization algorithm used to minimize performance function by iteratively moving in the direction of steepest descent as defined by the negative of the gradient. For the performance function defined in equation (7), steepest descent is defined as

(12) $$\theta_{n+1} = \theta_n - \frac{\mu}{2}\frac{\partial J}{\partial\theta_n}$$

The instantaneous gradient is derived as

(13) $$\frac{\partial J}{\partial\theta_n} = 2\left(\frac{\partial z_n}{\partial\theta_n}\right)^T W_z z_n + 2W_\theta\theta_n + 2W_{\Delta\theta}\Delta\theta_n = 2(T^T W_z z_n + W_\theta\theta_n + W_{\Delta\theta}\Delta\theta_n)$$

Then, control command update equation can be expressed as

(14) $$\theta_{n+1} = \theta_n - \mu(T^T W_z z_n + W_\theta\theta_n + W_{\Delta\theta}\Delta\theta_n)$$

where, $\mu > 0$ is adaptive rate, step size or learning rate.

## 3. VIBRATION CONTROL SIMULATION

### 3.1. Model Description

The HART (Higher harmonic Aeroacoustic Rotor Test) II rotor is used for the simulation. It is a 40 % dynamically scaled model of the Bo-105 hingeless rotor. The newly measured structural properties of the HART II blades [21] are used in the current model. Table 1 summarizes the main properties of the HART II rotor used in the analysis.

Table 1. Rotor properties.

| Properties | Values |
|---|---|
| Airfoil | NACA23012 |
| No. of blades (*N*) | 4 |
| Radius (*R*) | 2 m |
| Chord (*c*) | 0.121 m |
| Rotor speed (Ω) | 1041 rpm |
| Rotating direction | CCW |
| Solidity ($\sigma$) | 0.077 |

The comprehensive aeromechanics analysis code CAMRAD II is used to simulate the helicopter model. The blade structure is discretized into 16 nonlinear beam finite elements with each having 15 degrees-of-freedom which contain the contribution of rigid and elastic blade motions. The aerodynamic model used is based on the ONERA EDLIN unsteady theory with C81 airfoil table lookup. For the aerodynamics computation, the blade is divided into 17 aerodynamic panels. A rolled-up free vortex wake representation is used to compute the non-uniform induced velocities around the rotor. The time resolution in the wind tunnel trim is set to 15 degree azimuth angle.

### 3.2. Flight Condition

The baseline (BL) test case of the HART II wind tunnel test is used as uncontrolled condition. Wind speed of 33 m/s ($\mu$ = 0.15) and shaft angle of the



Presented at 47th European Rotorcraft Forum, United Kingdom, 7-9th September, 2021

isolated rotor system is 4.5 degree. The trim target has been specified as the same as the measured condition; $T = 3300\,N$ , $M_x = -20\,Nm$ , and $M_y = -20\,Nm$.

### 3.3. Twist Actuation

The top and bottom surfaces are covered by MFC actuators that are excited by electric fields to generate twist moments, and thus elastic twist deformations. Modeling of these active elements are not possible in CAMRAD II. Thus, twist moment induced by the actuators are used in CAMRAD II modeling and simulation as shown in Figure 4. It is assumed that the MFC actuator is embedded in the skin of the blade structure over 24% to 97% of the blade radius.

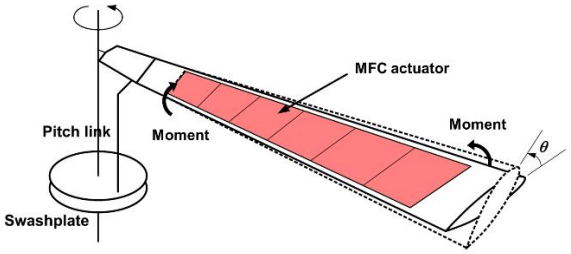


Figure 4. Mechanism of twist actuation.

External moments at the boundaries of the active element region on a blade is modeled representing active twist actuations. The voltage control law is defined as

(15) $$A(V) = A_0 + A_m \cos(m\psi - \phi)$$

where, $A_0$ is static voltage offset, $A_m$ is the actuation voltage amplitude, $\psi$ is azimuth angle, $\phi$ is the actuation phase angle, and $m$ denotes the $m$-th harmonics. Nose-up moment is produced by applying positive voltage input. The relationship between applied voltage and the twisting moment was set similarly to the MFC performance in Ref. 9, and 0.005 Nm/V is used in this study. The operating voltage range of the MFC actuator is also taken from Ref. 9, with voltage offset and maximum amplitude of 300 V and 800 V respectively. Applying a maximum amplitude of 800 V, which corresponds to a 4 Nm moment, to a CAMRAD II model blade in a non-rotating condition produces a 2.23 ° twist angle at the blade tip as shown in Figure 5.

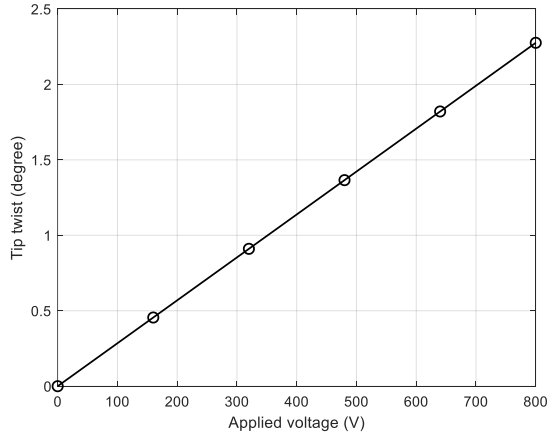


Figure 5. Blade tip twist response of the CAMRAD II model with respect to voltage control input.

### 3.4. Basis Data Generation

For the simulation of multicyclic vibration control of HART II BL condition, the response output vector $z$ and control input vector $\theta$ should be defined. And sets of input-output data as well as uncontrolled response is necessary. Because HART II has four blades, 4P nonrotating hub forces and moments are selected as output vector.

(16) $$z = [F_{x,4c}\ F_{y,4c}\ F_{z,4c}\ M_{x,4c}\ M_{y,4c}\ M_{z,4c}\ F_{x,4s}\ F_{y,4s}\ F_{z,4s}\ M_{x,4s}\ M_{y,4s}\ M_{z,4s}]^T$$

For multicyclic control input, 2P, 3P, 4P harmonics are utilized in the present simulation.

(17) $$\theta = [cos2P\ sin2P\ cos3P\ sin3P\ cos4P\ sin4P]^T$$

Table 2. Data generation cases.

| No. | Description | Actuation: $A(V) = A_0 + A_m \cos(m\psi - \phi)$ | | | |
|---|---|---|---|---|---|
| | | $A_0$ | $A_m$ | $m$ | $\phi$ |
| 1 | BL | 0 | 0 | 0 | 0 |
| 2 | BL offset | 300 V (1.5 Nm) | 0 | 0 | 0 |
| 3 | 2C20 | | 160 V (0.8 Nm) (20 %) | 2 | 0 |
| 4 | 2S20 | | | 2 | 90 |
| 5 | 3C20 | | | 3 | 0 |
| 6 | 3S20 | | | 3 | 90 |
| 7 | 4S20 | | | 4 | 0 |
| 8 | 4S20 | | | 4 | 90 |
| 9 | 2C40 | | 320 V (1.6 Nm) (40 %) | 2 | 0 |
| 10 | 2S40 | | | 2 | 90 |
| 11 | 3C40 | | | 3 | 0 |
| 12 | 3S40 | | | 3 | 90 |
| 13 | 4S40 | | | 4 | 0 |
| 14 | 4S40 | | | 4 | 90 |
| 15 | 2C60 | | 480 V (2.4 Nm) (60 %) | 2 | 0 |
| 16 | 2S60 | | | 2 | 90 |
| 17 | 3C60 | | | 3 | 0 |
| 18 | 3S60 | | | 3 | 90 |
| 19 | 4S60 | | | 4 | 0 |
| 20 | 4S60 | | | 4 | 90 |
| 21 | 2C80 | | 640 V (3.2 Nm) (80 %) | 2 | 0 |
| 22 | 2S80 | | | 2 | 90 |
| 23 | 3C80 | | | 3 | 0 |
| 24 | 3S80 | | | 3 | 90 |
| 25 | 4S80 | | | 4 | 0 |
| 26 | 4S80 | | | 4 | 90 |



Presented at 47th European Rotorcraft Forum, United Kingdom, 7-9th September, 2021

BL case, BL case with offset voltage, and 24 data sets with 6 independent twist actuations (*cos2P*, *sin2P*, *cos3P*, *sin3P*, *cos4P*, *sin4P*) with 20%, 40%, 60%, 80% amplitudes have been generated with the same trim target. The twist actuation applied in each case is shown in Table 2.

### 3.5. Offline System Identification

The system model $\hat{T}$ is obtained by using equation (6). For the system using 2P, 3P, and 4P harmonics as control inputs, 24 data sets from case 3 to 26 defined in Table 2 were used. The input matrix is

(18) $\Theta = [\theta_1\ \theta_2\ \ldots\ \theta_7\ \ldots \theta_{24}]$

where, $\theta_1 = [0.2\ 0\ 0\ 0\ 0\ 0]^T$, $\theta_2 = [0\ 0.2\ 0\ 0\ 0\ 0]^T$, ... , $\theta_7 = [0.4\ 0\ 0\ 0\ 0\ 0]^T$ , ... , $\theta_{24} = [0\ 0\ 0\ 0\ 0\ 0.8]^T$ (normalized control input, 1 = 800 V = 4 Nm). The response matrix *Z* is constructed by subtracting the uncontrolled response $z_0$ form the response $z$, because the measured response is the sum of the uncontrolled response and the generated response by the control input through the transfer function.

If the system is perfectly linear, data set with actuation amplitude variations are not necessary. Since the 6 control inputs are independent of each other, 6 sets of data are sufficient. For a single harmonic control case, 8 data sets were used, with 2 independent control inputs and 4 amplitude changes. Likewise, if the system is perfectly linear, the system model can be obtained from 2 data sets.

### 3.6. Control Simulation

Two kinds of open-loop control simulations have been performed to investigate vibration control performance. The one is linear system prediction using the identified system model, and the other is CAMRAD II calculation using the optimal control input as shown in Figure 6.

Similarly, closed-loop simulation was also performed in two ways as shown in Figure 7. At first, closed-loop

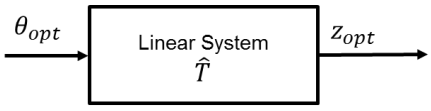


$$z_{opt} = z_0 + \hat{T}\theta_{opt}$$

(a) Linear system prediction


(b) CAMRAD II calculation with optimal input

Figure 6. Open-loop control simulation.

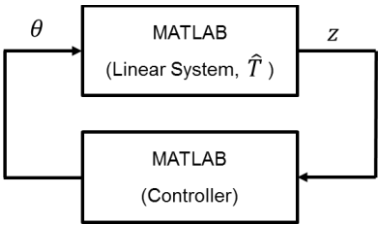


(a) Closed-loop simulation using the identified linear system

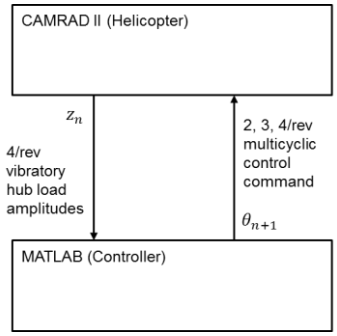


(b) MATLAB/CAMRAD II coupled closed-loop simulation

Figure 7. Closed-loop control simulation.

simulation using the identified linear system was performed to investigate the responses of the system with respect to the changes of learning rate. After selecting the learning rate, MATLAB/ CAMRAD II coupled simulation has been performed in the same way as loosely coupled CFD/CA analysis. 4P harmonics of the nonrotating hub load at the current time step are calculated in CAMRAD II and provided to MATLAB, then multicyclic control command is calculated using equation (14) and provided to CAMRAD.

### 3.7. Vibration Index

A nondimensionalized vibration index (VI) is defined to represent vibration reduction performance in a single number combining 12 output responses.

(19) $$VI = \frac{\sqrt{(F_{x,4})^2 + (F_{y,4})^2 + (F_{z,4})^2}}{W_0} + \frac{\sqrt{{M_{x,4}}^2 + {M_{y,4}}^2 + {M_{z,4}}^2}}{RW_0}$$

Here, $(F_{x,4})^2 = (F_{x,4C})^2 + (F_{x,4S})^2$, and forces and moments are nondimensiolalized by $W_0$ and $RW_0$ respectively.

## 4. RESULTS AND DISCUSSION

### 4.1. System Responses to Control Input

Multicyclic control of the helicopter vibration is based on the assumption of a linear, quasi-static, frequency



Presented at 47th European Rotorcraft Forum, United Kingdom, 7-9th September, 2021

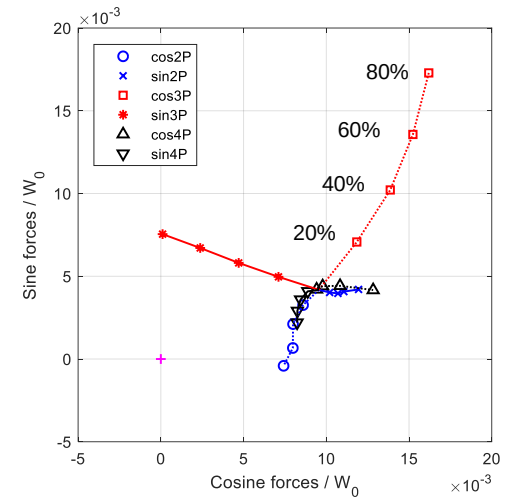


(a) $F_x$

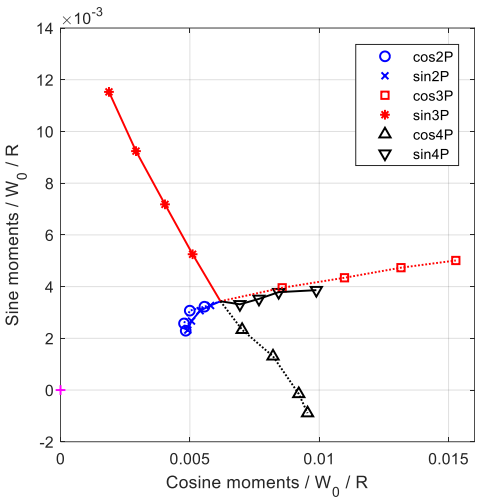


(d) $M_x$

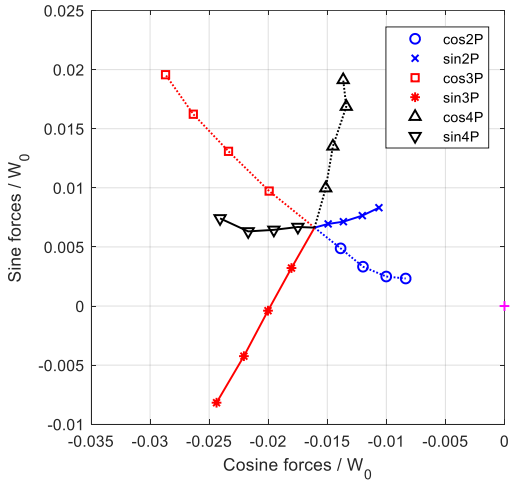


(b) $F_y$

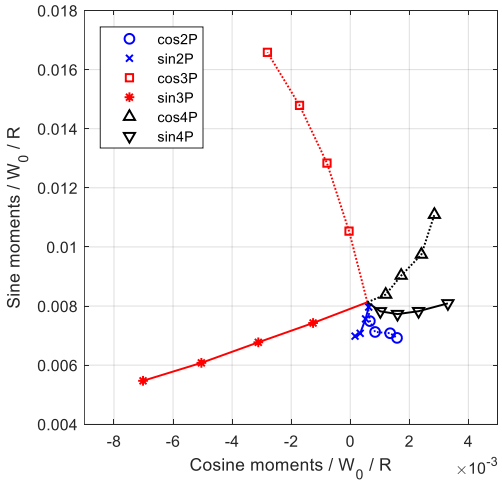


(e) $M_y$

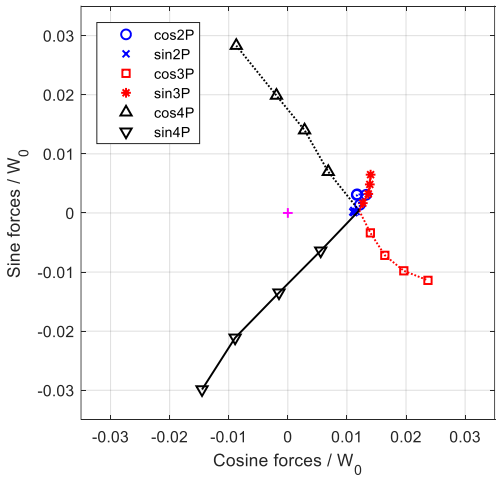


(c) $F_z$

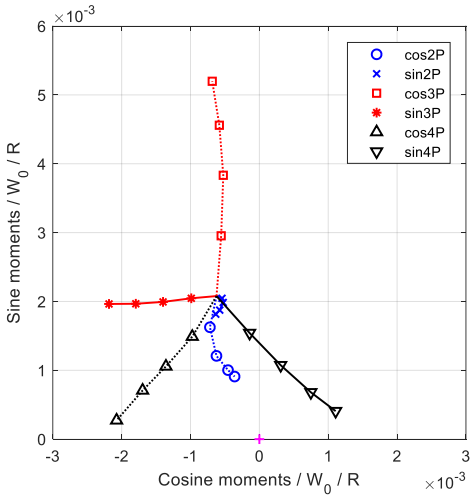


(f) $M_z$

Figure 8. Responses to independent control input.



Presented at 47th European Rotorcraft Forum, United Kingdom, 7-9th September, 2021

-domain representation of the helicopter. So, vibration control can be achieved when the system is linear. Therefore linearity of the helicopter system should be checked. If the following two characteristics are met, it is possible to generate controllable vibratory loads with arbitrary amplitudes and directions.

(1) The magnitude of the vibratory loads generated by the independent control input should be proportional to the amplitudes of actuation.

(2) The vibratory loads due to cosine harmonic excitation and the vibratory loads due to sine harmonic excitation should have 90 degree phase difference.

Nonrotating hub force and moment changes according to the independent control input with amplitude variations are shown in Figure 8. For 2P actuation, the response of $F_x$ and $F_y$ seems to increase proportionally as the excitation amplitude increases. The phase differences of the $F_x$ and $F_y$ changes according to cosine and sine harmonic inputs are not 90 degrees, but it seems that it is possible to generate vibratory loads having an arbitrary magnitude and direction by using the two responses as basis vectors. Other hub load components, $F_z$, $M_x$, $M_y$, and $M_z$ show a large nonlinearity, which makes it difficult to predict, but the magnitudes of the responses are relatively small, so the influence on control is expected to be small. For 3P actuation, all 6 hub vibratory loads show the responses proportional to the actuating amplitudes, and the phase differences are close to 90 degrees. Only the $F_z$ response shows that it is slightly less sensitive to sin3P excitation. The overall responses seem to be good for generating controllable vibratory loads to cancel the unwanted vibration. The response to 4P actuation seems better than 2P case and worse than 3P case. However, for the $F_z$ response, the case of 4P actuation seems to be the most linear and effective, and the $M_z$ response is also very linear.

Overall, it is not a perfect linear system, but it is expected that the vibration control utilizing the vibration generated by multicyclic twist actuation is possible. In the case of $F_x$, $F_y$, $M_x$, and $M_y$, the vibration generated by the 3P actuation expected to be useful, and in the case of $F_z$ and $M_z$, the vibration generated by the 4P actuation is expected to be effective.

### 4.2. Open-loop Control

Seven combinations of multicyclic open-loop control have been simulated. For the calculation of optimal control input, $W_z = I$ and $W_{\Delta\theta} = 0$ have been used. Initially, $W_\theta = 0$ was also applied, but when the optimal solution exceeded the operating range of the MFC actuator, $W_\theta = a \times I$ $(a > 0)$ was applied to limit the actuation voltage within the allowable range. The performance of each multicyclic control cases are summarized in Table 3.

Table 3. Vibration reduction performances of multicyclic control.

| Case | $a$ $(W_\theta = aI)$ | VI reduction (prediction) | VI reduction (CAMRAD II) | VI reduction difference (CAMRAD II – prediction) |
|---|---|---|---|---|
| BL | - | - | - | |
| BL offset | - | - | 7% | |
| 2P | 2000 | 37% | 29% | 9% |
| 3P | 0 | 51% | 55% | -4% |
| 4P | 0 | 9% | 10% | -1% |
| 2P+3P | 1000 | 55% | 55% | 0% |
| 2P+4P | 3000 | 42% | 29% | 14% |
| 3P+4P | 0 | 58% | 64% | -6% |
| 2P+3P+4P | 900 | 66% | 57% | 10% |

It can be seen that even if only the offset voltage is applied to the BL case, there is a 7% vibration reduction effect. For single harmonic control, 3P actuation case shows the maximum vibration reduction performance. For multiple harmonic control, vibration reduction performances are excellent for 2P+3P, 3P+4P, and 2P+3P+4P including 3P actuation. In the linear system prediction, 2P+3P+4P case was expected to have the best vibration reduction performance, but CAMRAD II calculation result shows that 3P+4P case is slightly better than 2P+3P+4P case. Due to the nonlinearity, the CAMRAD II calculation results are slightly different from the linear system prediction. Especially, it can be seen that the difference is relatively large when the 2P harmonic, which shows relatively higher nonlinearity than other harmonics, is included in the control input.

Figure 9 shows the optimal control input for the cases including 3P harmonic actuation. The waveforms for 3P and 3P+4P cases are similar and

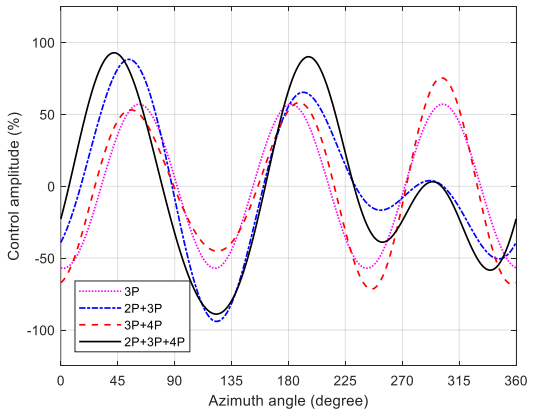


Figure 9. Optimal multicyclic control solutions of multicyclic.



Presented at 47th European Rotorcraft Forum, United Kingdom, 7-9th September, 2021

the waveforms for 2P+3P and 2P+3P+4P are very close. The big difference between these two groups is the actuation around 300 degree of the azimuthal position. 3P and 3P+4P cases have inputs of similar amplitude as before, but the control inputs are greatly reduced to around 0 in cases of 2P+3P and 2P+3P+4P.

Figure 10 shows the hub load components from linear system prediction and CAMRAD II calculations for the cases including 3P harmonic actuation. Although the linear system prediction result is slightly different from the CAMRAD II calculation result, but it can be seen that the overall vibration characteristics are well estimated. One thing to note here is that the VI reduction performance is similar for these 4 multicyclic controls, but the vibration reduction performance for each load components is different. A 55% VI reduction performance can be achieved with 3P single harmonic actuation, but the $F_z$ reduction effect is not significant. On the other hand, in the case of 3P+4P or 2P+3P+4P multicyclic control, it can be seen that all load components are reduced. If it is required to reduce a specific load component relatively much more, it is possible to use a larger weight for the specific load component in the response weighting matrix $W_z$.

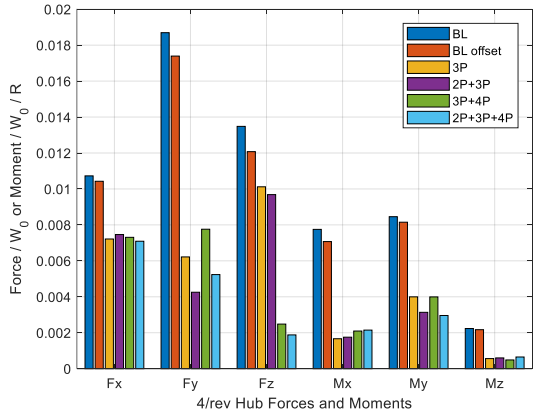


(a) Linear system prediction

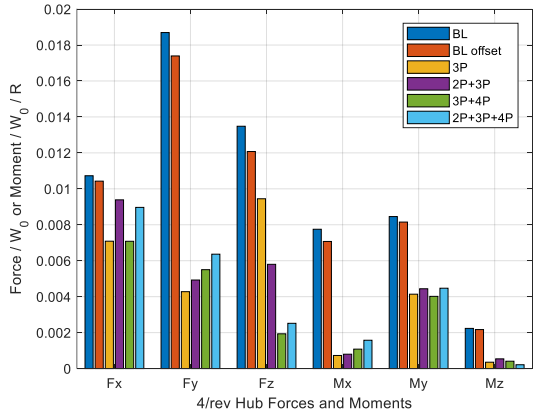


(b) CAMRAD II calculation

Figure 10. Nonrotating hub load responses to multicyclic control inputs.

### 4.3. Comparison with Single Harmonic Control with Magnitude & Phase Sweep

The optimal solutions for single harmonic actuations are shown in Table 4. These results can be compared to conventional amplitude and phase sweep approach. Amplitude and phase sweep has been performed by applying 4 amplitude changes (20%, 40%, 60%, and 80%) and control phase change in 30 degree step for 2P, 3P and 4P excitation frequencies. Figure 11, Figure 12, and Figure 13 show the results of magnitude and phase sweep. Optimal control input results are also displayed. It can be seen that the case of applying the control input obtained by multicyclic optimal control is very close to the minimum vibration condition obtained by amplitude and phase sweep. Although similar minimum vibration conditions can be obtained through the optimal control technique or the amplitude and phase sweep method, the number of calculations required for each method is greatly different. In the case of magnitude and phase sweep with 4 amplitudes and 30 degree phase steps, total 48 conditions for a single harmonic input have been

Table 4. Optimal solutions for single harmonic control input.

| Case | Optimal solution | | Optimal solution | |
|---|---|---|---|---|
| | Cos (%) | Sin (%) | Mag. (%) | Phase (deg) |
| 2P | 79.5 | 51.0 | 94.5 | 32.7 |
| 3P | -56.8 | -5.9 | 57.1 | 185.9 |
| 4P | 4.5 | 8.4 | 9.5 | 61.9 |

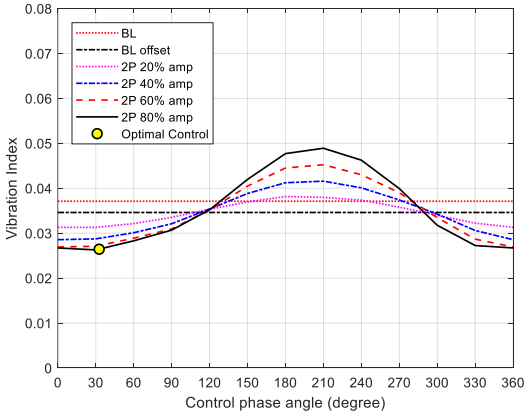


Figure 11. Vibration reduction comparison for 2P excitation.



Presented at 47th European Rotorcraft Forum, United Kingdom, 7-9th September, 2021

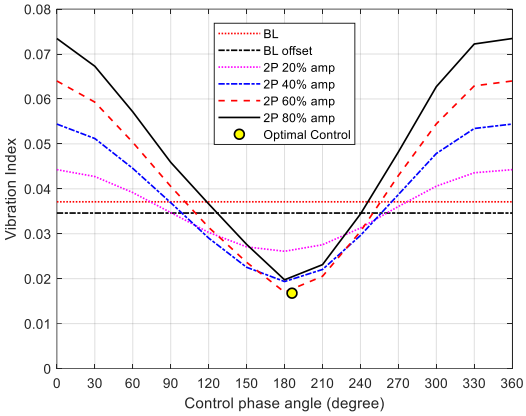


Figure 12. Vibration reduction comparison for 3P excitation.

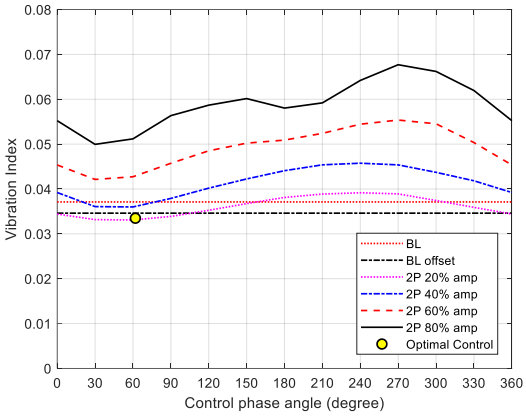


Figure 13. Vibration reduction comparison for 4P excitation.

calculated. On the other hand, in the case of optimal control, 8 data sets are required for system identification including 4 amplitude changes to 2 independent control inputs ( $cos\mathrm{NP}$ and $sin\mathrm{NP}$ ). Including uncontrolled case and the case for evaluating the optimal control input, a total of 10 data set are required. The minimum vibration condition can be found very effectively through the optimal control technique.

If the same amplitude and phase sweep approach are applied for 2 harmonic inputs with 4 amplitude changes and 30 degree phase steps, analyses should be performed for 2304 combinations. For multicyclic optimal control, 16 excitation cases and 1 uncontrolled case are sufficient for producing the optimal solution for the minimum vibration. Including the evaluation of the optimal control, 18 data sets are required. As the number of control harmonics increases, the number of calculations required for the amplitude and phase sweep method increases exponentially, but the number of calculations required for the multicyclic optimal control increases arithmetically.

### 4.4. Blade Tip Deformations

Looking at the blade tip elastic flap deformation in BL condition, a large lateral flapping in 1/rev is observed in Figure 14. Even if an offset voltage is applied, the flap elastic deformation is almost the same as the BL condition because it is trimmed at the same thrust. When the multicyclic optimal control inputs are applied, the maximum flap deflections are approximately the same, but the waveforms change. The waveforms for 3P and 3P+4P cases are similar and the waveforms for 2P+3P and 2P+3P+4P are very close. This appears to be the result of similar control input waveforms for both groups as shown in Figure 9.

When an offset voltage is applied to the BL condition, the blade tip elastic torsion shifts without changing the waveform as shown in Figure 15. The linear twist distribution of the blade is reduced by the offset voltage, so the collective pitch angle required for trim is reduced, resulting in the overall shift of the elastic

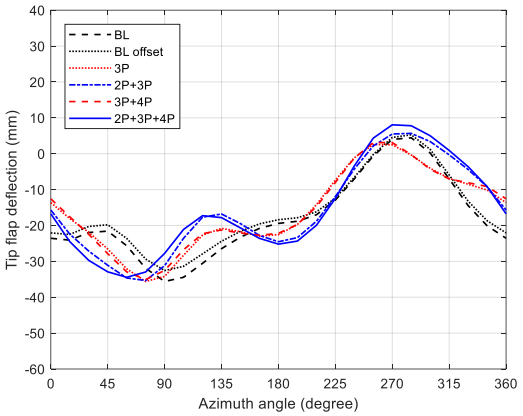


Figure 14. Blade tip deflections.

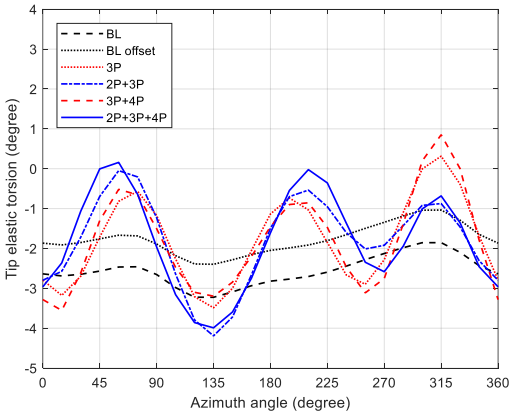


Figure 15. Blade tip elastic torsion.



Presented at 47th European Rotorcraft Forum, United Kingdom, 7-9th September, 2021

torsional deformation. When multicyclic control inputs are applied, the elastic torsional deflection look very similar to the control input waveform. Like the control input and flap deformation, it can be divided into two groups. For 2P+3P and 2P+3P+4P cases, it can be seen that the elastic deformations are also smaller than 3P and 3P+4P cases, because smaller control inputs are provided at around 300 degree azimuthal position.

### 4.5. Closed-loop Control

Closed-loop control simulation has been performed for the case of using the 2P+3P+4P control input. The same system model $\hat{T}$ and weight matrices $W_z$, $W_\theta$, and $W_{\Delta\theta}$ used for open-loop control were used.

When applying a gradient descent algorithm, one of the most important thing is the selection of the learning rate $\mu$. Initial guessing for the order of magnitude of the learning rate can be done using the optimal solution and the instantaneous gradient value at the first time step. Then, a closed-loop simulation using the identified linear system was performed to investigate the responses of the system with respect to the changes of learning rate as shown in 16. As $\mu$ increases from 0.000005 to 0.00002, the speed of convergence increases significantly. When $\mu$ is 0.00002, the almost lowest level of VI can be achieved within 5 time steps. However, increasing $\mu$ from 0.00002 to 0.00005 slows down the system response. This is because the control command is fluctuating due to large learning rate. If $\mu$ increases further and goes above 0.000053, the system diverges. When $\mu$ = 0.00001, the speed of the system response appears to be moderate, and the MATLAB/CAMRAD II coupled simulation has been performed using this value.

Figure 17 shows the simulation results of vibration reduction performance from time steps 0 to 16. MATLAB/ CAMRAD II coupled simulation result is very close to the linear system prediction result. Vibration is reduced to near the optimum response level within 15 time steps. The time history of the control command calculated by MATLAB/CAMRAD II coupled simulation shows a very good correlation with the linear system prediction as shown in Figure 18. In the Figure, lines and markers represent the linear system simulation results and the MATLAB/CAMRAD II coupled simulation results, respectively.

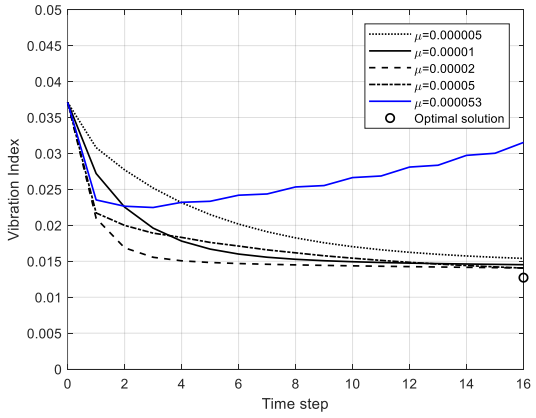


Figure 16. Vibration reduction performance according to learning rate.

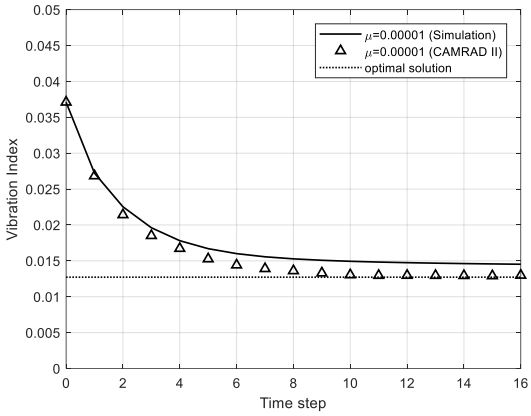


Figure 17. Vibration reduction performance calculated by MATLAB/CAMRAD II coupled simulation.

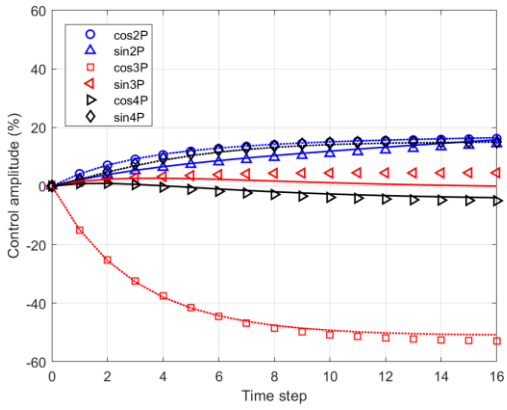


Figure 18. Control command history calculated by MATLAB/CAMRAD II coupled simulation.

The advantage of closed-loop control is that $\mu$ can be used to control the speed of the system response. Adjusting $\mu$ allows the control input to change smoothly and not abruptly, so that minimum vibration condition can be reached without applying excessive load on the actuators. And control commands converge to an open-loop optimal solution as time step increases.



Presented at 47th European Rotorcraft Forum, United Kingdom, 7-9th September, 2021

## 5. CONCLUSIONS

Open-loop and closed-loop vibration control of a helicopter rotor using multicyclic control technique has been investigated. Conclusions made for the current multicyclic vibration control simulation are as follows:

1) Although the artificial flight data for a descent flight condition generated using CAMRAD II are not perfectly linear, it is possible to apply linear optimal control strategy.

2) Vibration is reduced by applying a static nose-up twist actuation in descent flight condition.

3) Multicyclic optimal control technique can find low vibration conditions with fewer calculations compared to exhaustive testing methods such as amplitude and phase sweep.

4) Better vibration suppression performance can be obtained with multiple harmonic inputs compared to using a single harmonic input.

5) When optimal control inputs are applied, the blade tip flap deflections do not change significantly, but the blade tip elastic torsions show behaviors similar to the control input waveforms.

6) MATLAB/CAMRAD II coupled closed-loop simulation result is close to linear system prediction result. Therefore, a closed-loop controller design can be performed through linear system simulation.

## 6. ACKNOWLEDGEMENT

This study has been supported by Korea Aerospace Research Institute's R&D program funded by the Ministry of Science and ICT, Republic of Korea (Project Numbers: FR21A05, FR21P31).

## 7. REFERENCES

[1] Gmelin, B.L., Heller, H., Mercker, E., Philippe, J.J., Preisser, J.S., and Yu, Y.H., "The HART Programme - A Quadrilateral Cooperative Research Effort," American Helicopter Society 51st Annual Forum Proceedings, Fort Worth, TX, USA, May 9-11, 1995.

[2] Kessler, C., "Active Rotor Control for Helicopters: Motivation and Survey on Higher Harmonic Control," 36th European Rotorcraft Forum Proceedings, Paris, France, Sep. 7-9, 2010.

[3] Kessler, C., "Active Rotor Control for Helicopters: Individual Blade Control and Swashplateless Rotor Designs," 36th European Rotorcraft Forum Proceedings, Paris, France, Sep. 7-9, 2010.

[4] Jacklin, S.A., Blaas, A., Swanson, S.M., and Teves, D., "Second Test of a Helicopter Individual Blade Control System in the NASA Ames 40-by-80 feet Wind Tunnel," American Helicopter Society 2nd International Aeromechanics Specialists Conference Proceedings, Bridgeport, CT, Oct. 11-13, 1995.

[5] Straub, F.K., Anand, V.R., Lau, B.H., and Birchette, T.S., "Wind Tunnel Test of the SMART Active Flap Rotor," *Journal of the American Helicopter Society*, Vol. 63, (1), Jan. 2018, pp. 1-16, DOI: 10.4050/JAHS.63.012002

[6] Dieterich, O., Rabourdin, A., Maurice, J.-B., and Konstanzer P., "Blue PulseTM: Active Rotor Control by Trailing Edge Flaps at Airbus Helicopter," 41st European Rotorcraft Forum Proceedings, Munich, Germany, Sep. 1-4, 2015.

[7] Wilbur, M.L., Mirick, P.H., Yaeger Jr., W.T., Langston, C.W., Cesnik, C.E.S., and Shin, S., "Vibratory Loads Reduction Testing of the NASA/ARMY/MIT Active Twist Rotor," American Helicopter Society 57th Annual Forum Proceedings, Washington, DC, USA, May 9-11, 2001.

[8] Hoffmann, F., Opitz, S., and Riemenschneider, J., "Validation of Active Twist Modeling on Whirl Tower Tests," American Helicopter Society 65th Annual Forum Proceedings, Graphvine, TX, USA, May 27-29, 2009.

[9] Lim, J. W., Boyd, D. D., Jr., Hoffmann, F., van der Wall, B. G., Kim, D.-H., Jung, S. N., You, Y. H., Tanabe, Y., Bailly, J., Lienard, C., and Delrieux, Y., "Aeromechanical Evaluation of Smart-Twisting Active Rotor," 40th European Rotorcraft Forum Proceedings, Southampton, U.K., Sep. 2-5, 2014.

[10] Kobiki, N., Tanabe, Y., Aoyama, T., Kim, D.-H., Kang, H.J., Wie, S.-Y., and Kim, S.-H., "Design, Analysis and Prototyping of Active Tab Rotor," *Transactions of the Japan Society for Aeronautical and Space Sciences*, Vol. 62, (2), March 2019, pp. 64-74, DOI: 10.2322/tjsass.62.64

[11] Büter, A. and Breitbach, E., "The Main Sources of Helicopter Vibration and Noise Emissions and Adaptive Concepts to Reduce Them," EUROMECH 341 Smart Structures and Materials, Giens, France, Sept. 1995.

[12] Kalow, S., Opits, S., Riemenschneider, J., and Hoffmann, F., "Results of a Parametric Study to



Presented at 47th European Rotorcraft Forum, United Kingdom, 7-9th September, 2021

Adapt Structural Properties and Strain Distribution of Active Twist Blades," American Helicopter Society 72th Annual Forum Proceedings, West Parm Beach, Florida, USA, May 17-19, 2016.

[13] Kalow, S., van de Kamp, B., Keimer, R., and Riemenschneider, J., "Next Generation Active Twist Helicopter Rotor Blade – Simulated Results Validated by Experimental Invetigation," 45th European Rotorcraft Forum Proceedings, Warsaw, Poland, Sep. 17-20, 2019.

[14] Zhang, Q., Hoffmann, F., van der Wall, B. G., "Benefit studies for rotor with active twist control using weak fluid-structure coupling", 35th European Rotorcraft Forum Proceedings, Hamburg, Germany, Sep. 22-25, 2009.

[15] Bailly, J., Delrieux, Y., "Improvement of noise reduction and performance for a helicopter model rotor blade by active twist actuation", 35th European Rotorcraft Forum Proceedings, Hamburg, Germany, Sep. 22-25, 2009.

[16] Fogarty, D.E., Wilbur, M.L., and Sekula, M.K., "The Effect of Non-harmonic Active Twist Actuation on BVI Noise," American Helicopter Society 67th Annual Forum Proceedings, Virginia Beach, VA, USA, May 3-5, 2011.

[17] Jain, R., Yeo, H., and Chopra, I., "Computational Fluid Dynamics-Computational Structure Dynamics Analysis of Active Control of Helicopter Rotor for Performance Improvement," *Journal of the American Helicopter Society*, Vol. 55, (4), Oct. 2010, pp. 1-14, DOI: 10.4050/JAHS.55.042004

[18] You, Y.H., and Jung, S.N., "Optimum active twist input scenario for performance improvement and vibration reduction of a helicopter rotor," Aerospace Science and Technology, Vol. 63, April 2017. Pp. 18-32, DOI: 10.1016/j.ast.2016.12.011

[19] Johnson, W., "Self-Tuning Regulators for Multicyclic Control of Helicopter Vibration," NASA TP 1996, 1982.

[20] Chopra, I., and McCloud, J. L., III, "A numerical Simulation Study of Open-Loop, Closed-Loop, and Adaptive Multicyclic Control Systems," *Journal of the American Helicopter Society*, Vol. 28, (1), Jan. 1983, pp. 63-77. DOI: 10.4050/JAHS.28.1.63.

[21] Jung, S.N., You, Y.H., Dhadwal, M.K., Riemenschneider, J., Hagerty, B.P., "Study on blade property measurement and its influence on air/structural loads," AIAA Journal, Vol. 53, (11), Nov. 2015, 3221–3232, DOI: 10.2514/1.J053686



Presented at 47th European Rotorcraft Forum, United Kingdom, 7-9th September, 2021